

Increases in tropical rainfall driven by changes in frequency of organized deep convection

Jackson Tan^{1†}, Christian Jakob¹, William B. Rossow² & George Tselioudis³

Increasing global precipitation has been associated with a warming climate resulting from a strengthening of the hydrological cycle¹. This increase, however, is not spatially uniform. Observations and models have found that changes in rainfall show patterns characterized as ‘wet-gets-wetter’^{1–7} and ‘warmer-gets-wetter’^{5,8,9}. These changes in precipitation are largely located in the tropics and hence are probably associated with convection. However, the underlying physical processes for the observed changes are not entirely clear. Here we show from observations that most of the regional increase in tropical precipitation is associated with changes in the frequency of organized deep convection. By assessing the contributions of various convective regimes to precipitation, we find that the spatial patterns of change in the frequency of organized deep convection are strongly correlated with observed change in rainfall, both positive and negative (correlation of 0.69), and can explain most of the patterns of increase in rainfall. In contrast, changes in less organized forms of deep convection or changes in precipitation within organized deep convection contribute less to changes in precipitation. Our results identify organized deep convection as the link between changes in rainfall and in the dynamics of the tropical atmosphere, thus providing a framework for obtaining a better understanding of changes in rainfall. Given the lack of a distinction between the different degrees of organization of convection in climate models¹⁰, our results highlight an area of priority for future climate model development in order to achieve accurate rainfall projections in a warming climate.

Changes in the hydrological cycle are of paramount importance to society. To improve the accuracy of projections of future precipitation, we need to understand the physical processes that underpin the observed and simulated changes in precipitation. In the tropics, these changes have been shown to follow a ‘wet-gets-wetter’^{1–7} or a ‘warmer-gets-wetter’^{5,8,9} pattern. Using global climate models, these patterns have been respectively attributed to thermodynamic^{1,4–7} and dynamic changes^{5,8,9} in the climate system. In observations, these changes explain the increase in rainfall over some tropical regions of convergence such as the Intertropical Convergence Zone (ITCZ)².

In addition to observed changes in rainfall, there is evidence from an analysis of satellite-derived cloud regimes that mesoscale organized deep convection has also increased in frequency tropics-wide over the past 27.5 years¹¹. The cloud regime involved has a signature of deep convection combined with an extensive stratiform cloud and precipitation area, as is typical for convection with a high degree of organization¹². Despite occurring only about 5% of the time, this organized deep convective regime is responsible for half the tropical rainfall^{13–15}, which is a testament to its extraordinary precipitation rate over a large area. What is unclear is whether the recent changes in precipitation are in any way related to changes in organized deep convection. Here we investigate this connection.

We make use of cloud regimes associated with precipitating convection derived through a cluster analysis of joint-histograms describing the distributions of cloud top pressures and optical thickness in 280 km × 280 km grid boxes at daily resolution from the International

Satellite Cloud Climatology Project^{16,17} (see Methods). These cloud regimes (also called weather states) constitute an objective categorization of the cloud field, and a subset of the regimes has been associated with precipitating convection^{12–15,18–21}. Mesoscale organized deep convection is represented by the cloud regime CR1 as diagnosed from its cloud signature of widespread stratiform anvils (Fig. 1)¹², similarity in geographical distribution to mesoscale convective systems²² (Extended Data Fig. 1), highly convective environments^{12,13,18–21}, and intense precipitation rates^{12–15} (Fig. 2). It is this cloud regime that has been found to increase in frequency¹¹ (Extended Data Fig. 2). There are two more regimes associated with precipitating convection, namely CR2 and CR3, but both have less cloud cover (Fig. 1), lower precipitation rates (Fig. 2) and less organized cloud structures than CR1 (refs 12–15). These two regimes contribute 35% of the total rainfall between 1998 and 2009, in contrast with 47% by CR1 (Fig. 2). When these three regimes are taken together, their tropics-wide frequency has decreased slightly (Extended Data Fig. 2). This indicates that there has been a change in the distribution of the types of deep convection in the tropics, with less organized states decreasing in frequency and compensating for the increase in the occurrence of organized deep convection.

To make the connection between cloud regime and changes in rainfall, we decompose the change in total precipitation ΔP at every location into

$$\Delta P = \sum_i \Delta f_i \bar{p}_i + \bar{f}_i \Delta p_i \quad (1)$$

where f_i is the monthly-mean frequency of regime CR*i* and p_i is the monthly-mean within-regime precipitation rate of CR*i*; that is, the precipitation when the regime is present averaged over the month. The overbar denotes the mean over the entire period. In this framework, $\Delta f_i \bar{p}_i$ represents the contribution to the change in precipitation due to a change in monthly-mean frequency of the regime, and $\bar{f}_i \Delta p_i$ quantifies the contribution due to a change in the monthly-mean precipitation within the regime. We calculate the changes in regime frequency and within-regime precipitation rate as differences between the first and second halves of the data record. Because the derivation of within-regime precipitation rate requires the availability of daily rainfall information, we begin our investigation with the Tropical Rainfall Measuring Mission (TRMM) 3B42 precipitation data set²³ from 1998 to 2009, before extending our findings to the full cloud regime data set (July 1983 to December 2009) by using the Global Precipitation Climatology Project (GPCP) version 2.2 monthly rainfall product²⁴. All data sets are interpolated to the ISCCP equal-area grid (see Methods).

Computing each term in equation (1) for each grid box enables us to examine the spatial distribution of the changes in precipitation and their association with cloud regime changes from 1998 to 2009. Monthly-mean precipitation shows changes of opposite sign in different regions, with increases in areas such as the Pacific ITCZ and the Tropical West Pacific, and decreases in the eastern Indian Ocean and south of the Pacific ITCZ (Fig. 3a). The spatial distribution of the contribution to changes in precipitation by changes in the frequency of organized deep

¹ARC Centre of Excellence for Climate System Science, School of Earth, Atmosphere and Environment, Monash University, Clayton, Victoria 3800, Australia. ²CREST Institute at the City College of New York, New York, New York 10031, USA. ³NASA Goddard Institute for Space Studies, New York, New York 10027, USA. [†]Present address: NASA Wallops Flight Facility, Wallops Island, Virginia 23337, USA.

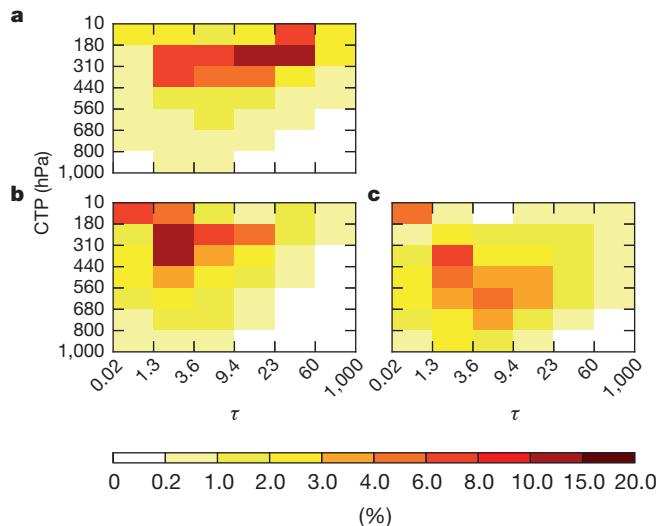


Figure 1 | Joint-histograms of the centroids of the convective cloud regimes. Cluster means (or centroids) of the convective cloud regimes in joint-histograms expressing the distribution of clouds in their cloud top pressure (CTP) and optical thickness (τ) of CR1 (a), CR2 (b) and CR3 (c). Bins in the top right area of the joint-histogram indicate clouds that are optically thick and have high tops, properties possessed by deep convective clouds. The cloud covers (sum over all bins) of the regimes are 95% (CR1), 90% (CR2) and 78% (CR3). The frequencies of the regimes over the entire period are 0.055 (CR1), 0.083 (CR2) and 0.142 (CR3).

convection ($\Delta f_i \bar{p}_i$) closely resembles the changes in mean rainfall (Fig. 3b), with a correlation of 0.69 and a root mean squared error of 0.34 (Extended Data Fig. 3a; see Methods). In contrast, the contribution from changes in the within-regime precipitation of CR1 ($\bar{f}_i \Delta p_i$) is mostly negative and bears little resemblance to observed changes in precipitation (Fig. 3c). The spatial correlation is only 0.19 and the root mean squared error is 0.49. This indicates that, when present, organized deep convection has produced less precipitation in the latter part of the analysis period than in the former. The contribution from the remaining two convective regimes captures the observed patterns of change in precipitation but is of much smaller magnitude, particularly in regions of increases in precipitation (Fig. 3d). In contrast, in regions of decreases in precipitation, the two unorganized convective regimes contribute about the same magnitude to the change as the organized regime does. When taken together, the three convective regimes largely reproduce observed changes in precipitation (Fig. 3e), confirming that deep convection is the major contributor to changes in tropical rainfall. These conclusions also hold when the GPCP daily precipitation data set²⁵ is used (Extended Data Fig. 4).

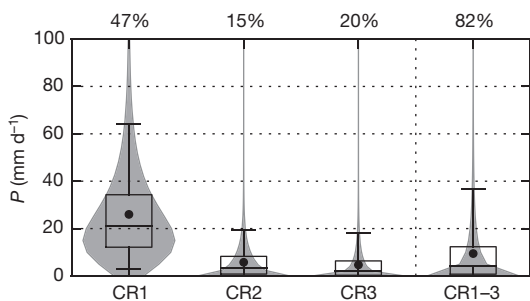


Figure 2 | Precipitation distributions of the convective CRs. Composites of daily precipitation from TRMM 3B42 with individual convective regimes (CR1, CR2 and CR3) as well as all convective regimes as one (CR1–3) between 1998 and 2009 in a ‘violin’ diagram, showing the mean (dot), median (horizontal line), interquartile range (box), 5th and 95th centiles (whiskers), and the probability distribution (grey ‘violin’). The numbers at the top show the percentage contribution to the total precipitation over the entire period.

The analysis of the cloud regimes above indicates that it is organized rather than unorganized precipitating convection that is involved in the observed increase in rainfall in the past decade. To confirm this result we turn to a data set independent of ISCCP. A characteristic of organized deep convection is that the stratiform component of rainfall is greater than the convective component¹². An increase in organized deep convection would therefore be identifiable through an increase in the area of stratiform precipitation as well as an increase in the relative contribution to the total precipitation by stratiform processes. The TRMM 3A25 data set²⁶ enables the calculation of both the stratiform rain area fraction f_{sa} and the stratiform rain rate fraction f_{sr} (see Methods). The spatial changes in both quantities show patterns similar to the change in total precipitation (Fig. 3f, g), especially over the oceans of the deep tropics (between about 15° N and 15° S). This confirms the conclusion reached in the analysis of the cloud regime, namely that an increase in tropical precipitation is a result of an increased frequency of organized deep convection.

Although instructive, the above analysis suffers from the lack of long-term daily precipitation observations over the oceans, which prevents a direct extension of the technique to the full period for which cloud regime data are available (July 1983 to December 2009) as a result of the inability to calculate p_i . We make an attempt at decomposing the changes in precipitation over the longer period by assuming that the values of p_i are equal to those of the shorter period (1998–2009). This enables us to calculate the contribution from changes in frequency of occurrence, $\Delta f_i \bar{p}_i$, of the three convective states for the full period to the longer-term changes in precipitation, for which we have monthly observations in the GPCP version 2.2 data set. This provides a first-order estimate of the relationship between change in precipitation and changes in the frequencies of various deep convective states.

The spatial distribution of the change in precipitation between July 1983 and December 2009 shares some similarity with the 1998–2009 period but has a smaller magnitude (Fig. 4a). An analysis of changes in rainfall for the shorter period using same data product shows that this disparity stems primarily from the difference in time period rather than the difference in data set. The contribution to the change in precipitation from the changes in frequency in organized deep convection alone, $\Delta f_i \bar{p}_i$, still shows similarities with the overall change in the wet regions (Fig. 4b), albeit with a lower correlation of 0.43 and a root mean squared error of 0.33 in contrast with the shorter period (Extended Data Fig. 3b). Using all three convective regimes once again adds detail in regions of decrease in rainfall (Fig. 4c), but it fails to represent the changes in precipitation in some regions, in particular over the Indian Ocean, where there was no geostationary satellite before 1998 (ref. 11), which may affect measurements of CR2 and CR3. It is worth noting that assuming the value of p_i derived from the shorter period is a strong assumption that is not necessarily justified. In addition, for the shorter period the changes in within-regime precipitation were negative, thereby compensating for some of the increases in precipitation from changes in frequency. Having to neglect those terms for the longer time period probably contributes to the overestimation of the magnitude of changes in precipitation. Nevertheless, qualitatively the results for the longer period confirm our assertion that the observed increase in the frequency of organized deep convection in the tropics is the main contributor to the increase in precipitation.

The finding that it is mainly the frequency of organized deep convection that contributed to the increase in precipitation in the tropics provides insights from an unconventional perspective to the question of whether changes in precipitation are dynamic^{5,8,9} or thermodynamic^{1,4–7} in origin. The frequency of organized deep convection is typically associated with the dynamics of the climate system such as the large-scale circulation^{13–15,18}. Indeed, there is a good spatial correspondence between changes in the dynamics of the tropical atmosphere, as reflected by large-scale mid-tropospheric vertical velocity, and that of organized deep convection (Extended Data Fig. 5). One can therefore argue that the changes in organized deep convection reflect a dynamic change in

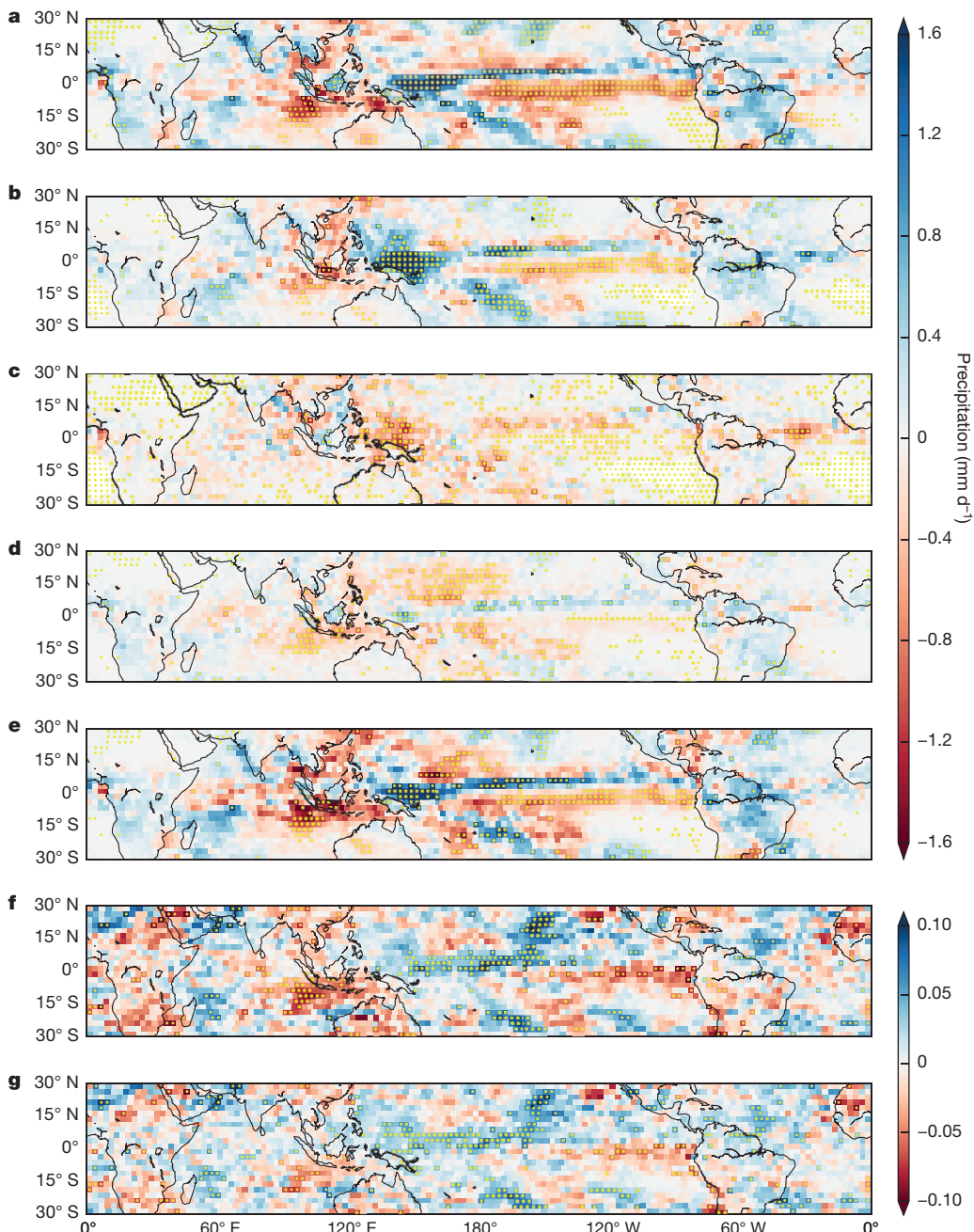


Figure 3 | The spatial distribution of the changes in precipitation from 1998 to 2009. **a**, Change in monthly-mean precipitation, ΔP . **b**, Contribution from the change in CR1 frequency, $\Delta f_1 \bar{P}_1$. **c**, Contribution from the change in within-CR1 rainfall, $\bar{f}_1 \Delta p_1$. **d**, Sum of the contributions from CR2 and CR3, $\Delta f_2 \bar{P}_2 + \bar{f}_2 \Delta p_2 + \Delta f_3 \bar{P}_3 + \bar{f}_3 \Delta p_3$. **e**, Sum of the contributions from all three convective regimes, $\sum_{i=1}^3 \Delta f_i \bar{P}_i + \bar{f}_i \Delta p_i$. **f**, **g**, Change in

stratiform area fraction, Δf_{sa} (**f**), and stratiform rain fraction, Δf_{sr} (**g**). Grid boxes with changes significant at $P < 0.1$ using the Monte Carlo permutation test are stippled, with the dots in yellow for visibility against dark backgrounds. See Extended Data Fig. 3a for correlations and root mean squared errors.

the climate system. This argument is strengthened by our finding that changes in within-regime precipitation of CR1, which are probably more characteristic of a thermodynamic response, have contributed mainly to a decline in precipitation.

If changes in precipitation are mediated through organized deep convection, this calls into question the ability of global climate models (GCMs) to predict changes in rainfall accurately, especially in extreme precipitation¹⁵. GCMs are currently unable to simulate any organized forms of deep convection, because convection is represented through an ensemble of unorganized buoyant plumes. This lack of organized deep convection is a well-known issue in GCMs¹⁰ and might well be a contributing factor to longstanding precipitation errors in models such

as the bias towards light rain. Model projections of precipitation are therefore made in the absence of a phenomenon prominent in the hydrological cycle. From our findings here, it is likely that this limitation in GCMs contributes to the disagreements⁴ between projected and observed changes in precipitation.

As a result of the inability of GCMs to represent organized deep convection, its effects are usually neglected in the analysis of precipitation projections. Given the societal importance of accurate precipitation projections in a warming climate, the role of organized deep convection in changes in precipitation identified in this study calls for a renewed effort to include a representation of convective organization in GCMs.

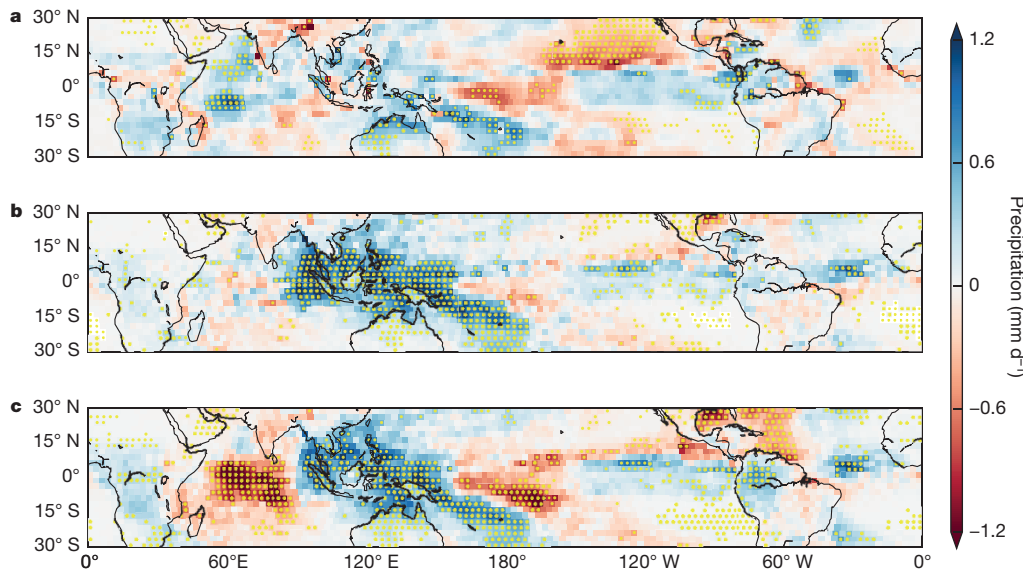


Figure 4 | The spatial distribution of the changes in precipitation from July 1983 to December 2009.
a, Change in monthly-mean precipitation, ΔP , from GPCP 2.2.
b, Contribution from the change in CRI frequency, $\Delta f_i \bar{p}_i$. **c**, Sum of the contributions from changes in the frequencies of the three convective regimes, $\sum_{i=1}^3 \Delta f_i \bar{p}_i$. The mean within-regime precipitation \bar{p}_i is assumed to be equal to that of TRMM 3B42. See the legend to Fig. 3 on stippling, and Extended Data Fig. 3b for correlations and root mean squared errors. Note the difference in the range of the colour scale from that in Fig. 3.

Online Content Methods, along with any additional Extended Data display items and Source Data, are available in the online version of the paper; references unique to these sections appear only in the online paper.

Received 23 September 2014; accepted 11 February 2015.

1. Held, I. M. & Soden, B. J. Robust responses of the hydrological cycle to global warming. *J. Clim.* **19**, 5686–5699 (2006).
2. Allan, R. P., Soden, B. J., John, V. O., Ingram, W. & Good, P. Current changes in tropical precipitation. *Environ. Res. Lett.* **5**, 025205 (2010).
3. Liu, C. & Allan, R. P. Multisatellite observed responses of precipitation and its extremes to interannual climate variability. *J. Geophys. Res.* **117**, D03101 (2012).
4. Chou, C. et al. Increase in the range between wet and dry season precipitation. *Nature Geosci.* **6**, 263–267 (2013).
5. Huang, P., Xie, S.-P., Hu, K., Huang, G. & Huang, R. Patterns of the seasonal response of tropical rainfall to global warming. *Nature Geosci.* **6**, 357–361 (2013).
6. Chou, C., Neelin, J. D., Chen, C.-A. & Tu, J.-Y. Evaluating the ‘rich-get-richer’ mechanism in tropical precipitation change under global warming. *J. Clim.* **22**, 1982–2005 (2009).
7. Seager, R., Naik, N. & Vecchi, G. A. Thermodynamic and dynamic mechanisms for large-scale changes in the hydrological cycle in response to global warming. *J. Clim.* **23**, 4651–4668 (2010).
8. Xie, S.-P. et al. Global warming pattern formation: sea surface temperature and rainfall. *J. Clim.* **23**, 966–986 (2010).
9. Chadwick, R., Boulte, I. & Martin, G. Spatial patterns of precipitation change in CMIP5: why the rich do not get richer in the tropics. *J. Clim.* **26**, 3803–3822 (2013).
10. Mapes, B. & Neale, R. Parameterizing convective organization to escape the entrainment dilemma. *J. Adv. Model. Earth Syst.* **3**, M06004 (2011).
11. Tselioudis, G., Tromer, E., Rossow, W. B. & Zerefos, C. S. Decadal changes in tropical convection suggest effects on stratospheric water vapor. *Geophys. Res. Lett.* **37**, L14806 (2010).
12. Jakob, C. & Schumacher, C. Precipitation and latent heating characteristics of the major Tropical Western Pacific cloud regimes. *J. Clim.* **21**, 4348–4364 (2008).
13. Tan, J., Jakob, C. & Lane, T. P. On the identification of the large-scale properties of tropical convection using cloud regimes. *J. Clim.* **26**, 6618–6632 (2013).
14. Lee, D., Oropoulopoulos, L., Huffman, G. J., Rossow, W. B. & Kang, I.-S. The precipitation characteristics of ISCCP tropical weather states. *J. Clim.* **26**, 772–788 (2013).
15. Rossow, W. B., Mekonnen, A., Pearl, C. & Goncalves, W. Tropical precipitation extremes. *J. Clim.* **26**, 1457–1466 (2013).
16. Jakob, C. & Tselioudis, G. Objective identification of cloud regimes in the Tropical Western Pacific. *Geophys. Res. Lett.* **30**, 2082 (2003).
17. Rossow, W. B., Tselioudis, G., Polak, A. & Jakob, C. Tropical climate described as a distribution of weather states indicated by distinct mesoscale cloud property mixtures. *Geophys. Res. Lett.* **32**, L21812 (2005).
18. Jakob, C., Tselioudis, G. & Hume, T. The radiative, cloud, and thermodynamic properties of the major tropical western Pacific cloud regimes. *J. Clim.* **18**, 1203–1215 (2005).
19. Li, W., Schumacher, C. & McFarlane, S. A. Radiative heating of the ISCCP upper level cloud regimes and its impact on the large-scale tropical circulation. *J. Geophys. Res. Atmos.* **118**, 592–604 (2013).
20. Stachnik, J. P., Schumacher, C. & Ciesielski, P. E. Total heating characteristics of the ISCCP tropical and subtropical cloud regimes. *J. Clim.* **26**, 7097–7116 (2013).
21. Handlos, Z. J. & Back, L. E. Estimating vertical motion profile shape within tropical weather states over the oceans. *J. Clim.* **27**, 7667–7686 (2014).
22. Laing, A. G. & Fritsch, J. M. The global population of mesoscale convective complexes. *Q. J. R. Meteorol. Soc.* **123**, 389–405 (1997).
23. Huffman, G. J. et al. The TRMM Multisatellite Precipitation Analysis (TMPA): quasi-global, multiyear, combined-sensor precipitation estimates at fine scales. *J. Hydrometeorol.* **8**, 38–55 (2007).
24. Adler, R. F. et al. The version-2 global precipitation analysis (1979–present). *J. Hydrometeorol.* **4**, 1147–1167 (2003).
25. Huffman, G. J. et al. Global precipitation at one-degree daily resolution from multisatellite observations. *J. Hydrometeorol.* **2**, 36–50 (2001).
26. Iguchi, T., Kozu, T., Meneghini, R., Awaka, J. & Okamoto, K. Rain-profiling algorithm for the TRMM precipitation radar. *J. Appl. Meteorol.* **39**, 2038–2052 (2000).

Acknowledgements. We thank S. Sherwood and B. Stevens for comments on the study. The GPCP combined precipitation data were developed and computed by the NASA/Goddard Space Flight Centre’s Mesoscale Atmospheric Processes Laboratory as a contribution to the GEWEX Global Precipitation Climatology Project, and provided by National Oceanic and Atmospheric Administration (NOAA) Office of Oceanic and Atmospheric Research and Earth System Research Laboratory Physical Sciences Division (PSD) at <http://www.esrl.noaa.gov/psd/>. The TRMM 3B42 and 3A25 data were provided by the NASA/Goddard Space Flight Center’s Mesoscale Atmospheric Processes Laboratory and Precipitation Processing System as a contribution to TRMM, and archived at the NASA Goddard Earth Sciences Data and Information Services Center. J.T. and C.J. are funded under the Australian Research Council Centre of Excellence for Climate System Science (CE110001028). W.B.R. is supported by NASA grant NNX13AO39G. G.T. acknowledges the support of the NASA Modeling Analysis and Prediction (MAP) programme managed by D. Considine. J.T. acknowledges support from the Monash University Postgraduate Publication Award.

Author Contributions J.T. and C.J. designed the study. J.T. conducted the analysis and obtained the results. C.J., W.B.R. and G.T. advised on the approach. J.T., W.B.R. and G.T. checked regime time series for satellite artefacts. All authors discussed the results and contributed to the preparation of the manuscript.

Author Information Reprints and permissions information is available at www.nature.com/reprints. The authors declare no competing financial interests. Readers are welcome to comment on the online version of the paper. Correspondence and requests for materials should be addressed to J.T. (jackson.tan@nasa.gov).

METHODS

Cloud regimes. The cloud regimes (or weather states) are derived from the International Satellite Cloud Climatology Project (ISCCP) D1 data set²⁷ using a *k*-means clustering algorithm applied to the daytime-averaged joint-histograms of cloud top pressure and optical thickness over grid boxes of 280 km × 280 km from July 1983 to December 2009 (refs 16, 17). The number of regimes is determined through an objective set of criteria¹⁷. When applied to grid boxes between ±35° latitudes, we obtain eight cloud regimes, three of which possess precipitating convective clouds in their centroids (CR1, CR2 and CR3). These eight regimes are highly similar to those in cloud regime studies using 3-hourly (but daytime-only) ISCCP joint-histograms²⁸. CR1 represents mesoscale organized deep convection according to its fingerprint of a large population of deep convective and thick stratiform anvil clouds, its extensive cloud cover, its geographical distribution and its precipitation characteristics. CR2 represents deep convection that is less organized in its nature, with some stratiform anvil as well as cirrus clouds. CR3 represents isolated deep convection with a larger abundance of shallower clouds that are suggestive of cumulus congestus, thus probably indicating a nascent phase of organized deep convection. The frequencies between ±35° latitudes of the regimes over the entire period are 0.055 (CR1), 0.083 (CR2) and 0.142 (CR3). These three convective regimes are very similar to those obtained in the deep tropics between ±15° latitudes¹⁷. All subsequent analyses are constrained to ±30° latitudes for consistency with other similar tropical precipitation studies^{2,3,6,9}.

Precipitation. For precipitation rates from 1998 to 2009, we use the 3-hourly Tropical Rainfall Measuring Mission (TRMM) version 7 Multisatellite Precipitation Analysis 3B42 product²³. For precipitation rates from July 1983 to December 2009, we use the Global Precipitation Climatology Project (GPCP) version 2.2 monthly rainfall product²⁴. For quantities on stratiform precipitation, we use the monthly TRMM version 7 3A25 product at 0.5° resolution²⁶. Stratiform rain area fraction is defined as the counts of non-zero estimated surface rain conditioned on stratiform rain divided by the counts of non-zero estimated surface rain. The stratiform rain rate fraction is defined as the mean of non-zero estimated surface stratiform rain rate divided by the mean of non-zero estimated total surface rain rate. Because precipitation rates are dependent on resolution, we coarsened the values to 2.5° resolution. Values in 3B42 are also first averaged over daytime to a daily resolution. All quantities are then linearly interpolated to the ISCCP equal-area grid (see <http://isccp.giss.nasa.gov/docs/mapgridinfo.html>). The GPCP One-Degree Daily (1DD) version 1.2 data set²⁵ (1997–2009) is also employed to verify the results from TRMM 3B42 (Extended Data Fig. 4).

Vertical velocity. Grid-mean vertical motion at 500 hPa for Extended Data Fig. 5 is obtained from the European Centre for Medium-Range Weather Forecasts Interim Re-Analysis data²⁹. The values are averaged from the 6 h intervals to a daily resolution and, as with precipitation, interpolated to the ISCCP grids.

Regime and changes in precipitation. Satellite artefacts in ISCCP have been known to affect the quantities of cirrus clouds detected³⁰, but cloud regimes are more robust against such artificial signals¹¹. This is confirmed by an absence of circular patterns indicative of satellite artefacts in the spatial distributions of the regression of frequency changes in each grid box to the overall frequency change. Furthermore, we

did not find any correspondence between sudden major changes in the frequency of CR1 and key satellite events or ancillary changes listed in the ISCCP metadata archives.

In calculating the change Δ , we take the difference between the means of the second half and the first half of the period. This option was chosen over least-squares linear regression because it conserves the relationship from $P = \sum_i f_i p_i$ to equation (1). Separate analyses using linear regression found no substantial differences from our results.

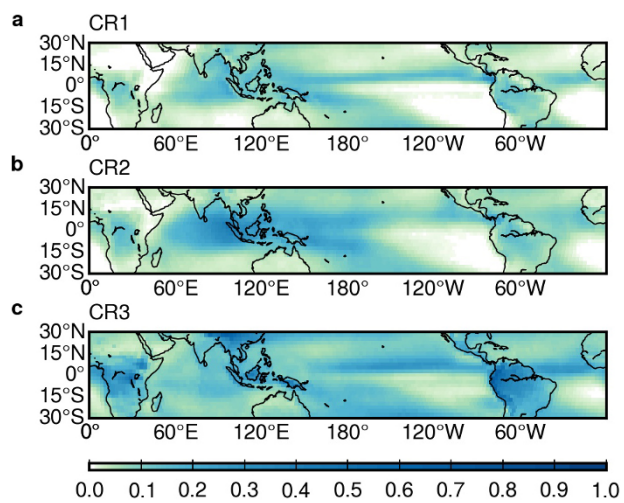
Spatial correlation and root mean squared error. Spatial correlation is the Pearson correlation of the two arrays representing the changes over the grid boxes. Because of the large number of grid boxes ($n = 3,298$), all correlations calculated are statistically significant at $P < 0.01$. However, the observed noise in the changes in precipitation can decrease a perfect correlation to between 0.72 and 0.79, derived from the average correlation ($n = 10,000$) between Δf and $\Delta f + N(0, \sigma_f / \mu_f \times \mu_{\Delta f})$, where f is the frequency of the variables, μ and σ are respectively the mean and standard deviation, and N is a Gaussian random noise. Root mean squared error is calculated by taking the square root of the mean of the square of the difference between two arrays. It captures the degree to which the two arrays are different in magnitude in each grid box, and is useful as a relative measure.

Statistical significance. The Monte Carlo permutation test was used to evaluate the statistical significance of the spatial distributions (Figs 3 and 4 and Extended Data Fig. 4), on the null hypothesis that the means of the two halves of the time period were the same. Each grid box was randomly permuted 10,000 times. Being non-parametric, this test is applicable for rainfall, which does not have a normal distribution.

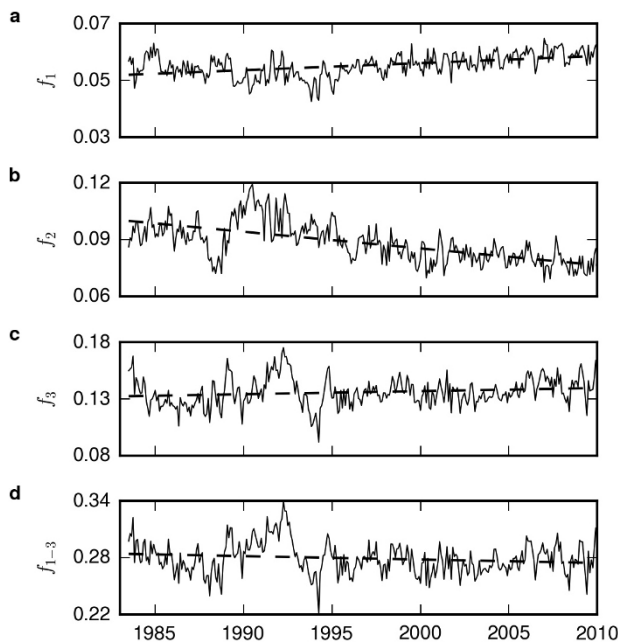
Data. The ISCCP D1 data set, from which the cloud regimes are derived, can be obtained following the instructions at <http://isccp.giss.nasa.gov/products/obtaining.html>. Both TRMM 3B42 and 3A25 can be downloaded from NASA PMM at <http://pmmm.nasa.gov/data-access/downloads/trmm>. GPCP 2.2 is available from NOAA PSD at <http://www.esrl.noaa.gov/psd/data/gridded/data.gpcp.html>, and GPCP 1DD can be downloaded from NOAA National Climatic Data Center at <http://www1.ncdc.noaa.gov/pub/data/gpcp/1dd-v1.2/>. ERA-Interim vertical velocity data can be downloaded from the European Centre for Medium-Range Weather Forecasts at <http://apps.ecmwf.int/datasets/>.

Code availability. All the codes used in the analysis in this paper and in the production of figures are available at https://github.com/JacksonTanBS/2015_Tan-et-al_Nature.

27. Rossow, W. B. & Schiffer, R. A. Advances in understanding clouds from ISCCP. *Bull. Am. Meteorol. Soc.* **80**, 2261–2287 (1999).
28. Oreopoulos, L. & Rossow, W. B. The cloud radiative effects of International Satellite Cloud Climatology Project weather states. *J. Geophys. Res.* **116**, D12202 (2011).
29. Dee, D. P. et al. The ERA-Interim reanalysis: configuration and performance of the data assimilation system. *Q. J. R. Meteorol. Soc.* **137**, 553–597 (2011).
30. Rossow, W. B., Walker, A. W. & Gardner, L. C. Comparison of ISCCP and other cloud amounts. *J. Clim.* **6**, 2394–2418 (1993).



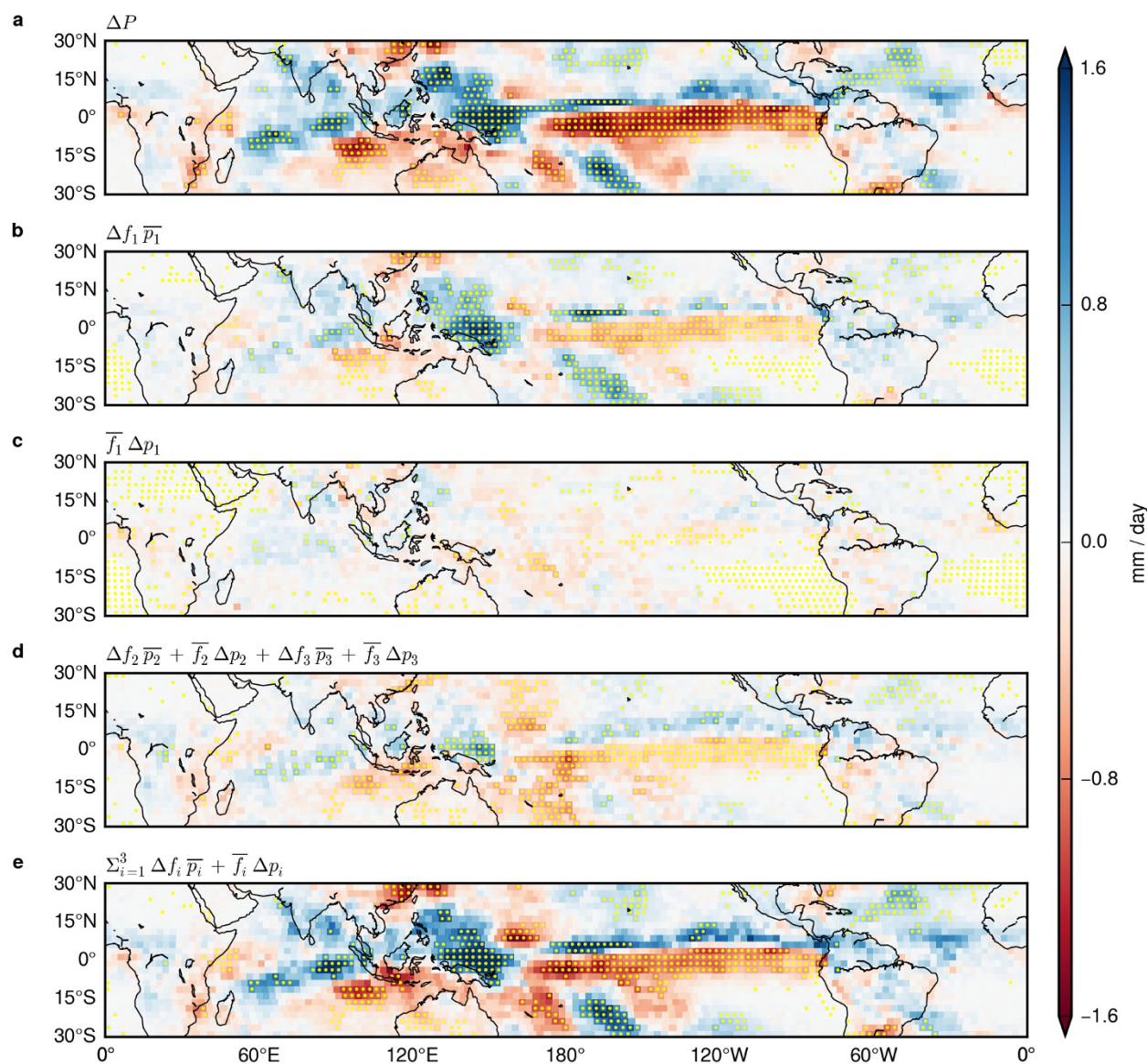
Extended Data Figure 1 | Geographical distribution of the convective cloud regimes. The frequency averaged over the entire period (July 1983 to December 2009) in each grid box for CR1 (a), CR2 (b), and CR3 (c).



Extended Data Figure 2 | Time series of the frequencies of the convective regimes. Monthly-mean frequencies of CR1 (a), CR2 (b) and CR3 (c), as well as the sum of all convective regimes CR1–CR3 (d) in the entire domain between $\pm 30^\circ$ latitudes (solid lines). The linear least-squares regression slopes are also shown (dashed lines). The differences in means between the two halves at two standard deviations (95%) are 0.0043 ± 0.0008 (a), -0.014 ± 0.002 (b), 0.003 ± 0.003 (c) and -0.006 ± 0.004 (d).

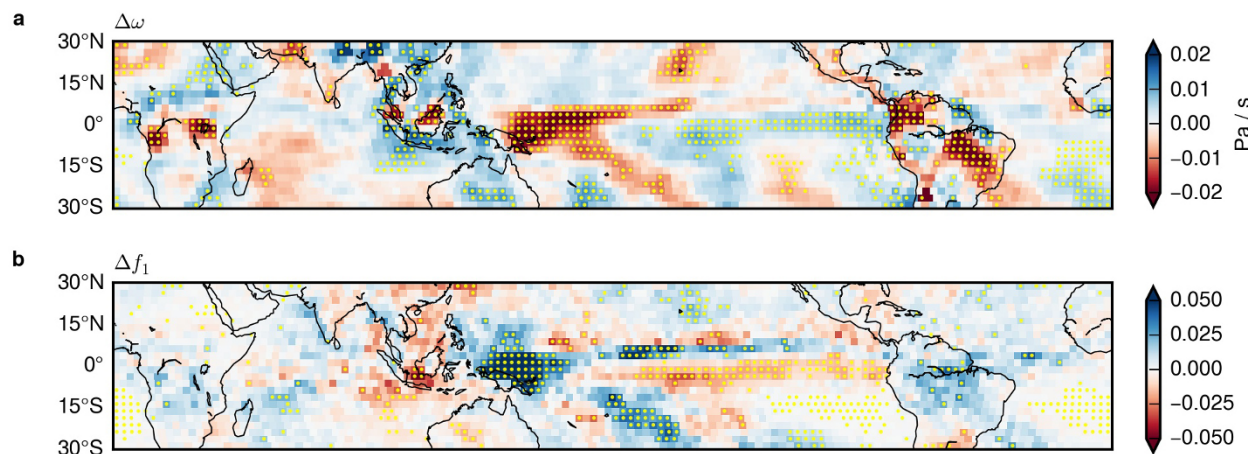
a	(b)	(c)	(d)	(e)	(f)	(g)
Fig. 3	0.69	0.19	0.51	0.85	0.37	0.31
correlation to (a)						
RMSE to (a)	0.34	0.49	0.39	0.26		
b	(b)	(c)				
Fig. 4	0.43	0.39				
correlation to (a)						
RMSE to (a)	0.33	0.38				
c	(b)	(c)	(d)	(e)		
Extended Data Fig. 4	0.80	0.40	0.69	0.90		
correlation to (a)						
RMSE to (a)	0.35	0.50	0.40	0.24		

Extended Data Figure 3 | Correlations and root mean squared errors of the spatial changes to change in total precipitation. Correlations and root mean squared errors with the first panel of the other panels in Fig. 3 (a), Fig. 4 (b) and Extended Data Fig. 4 (c).



Extended Data Figure 4 | The spatial distribution of the changes in precipitation from 1997 to 2009 using GPCP 1DD. **a**, Change in monthly-mean precipitation from GPCP 1DD. **b**, Contribution from the change in CR1 frequency. **c**, Contribution from the change in within-CR1 rainfall. **d**, Sum

of the contributions from the terms of CR2 and CR3. **e**, Sum of the contributions from the terms of all three convective regimes. See the legend to Fig. 3 on stippling, and Extended Data Fig. 3c for correlations and root mean squared errors.



Extended Data Figure 5 | Comparison between changes in organized deep convection and changes in dynamics from 1998 to 2009. **a**, Changes in grid-mean vertical motion at 500 hPa from ERA-Interim (negative is ascending motion). **b**, Changes in frequency of CR1.